Inorganic Chemistry

Article

pubs.acs.org/IC

Intracellular Distribution of Fluorescent Copper and Zinc Bis(thiosemicarbazonato) Complexes Measured with Fluorescence Lifetime Spectroscopy

James L. Hickey,[†,⊥] Janine L. James,[‡,§,⊥] Clare A. Henderson,[†,∥] Katherine A. Price,[‡,§] Alexandra I. Mot,[‡,§] Gojko Buncic,[†] Peter J. Crouch,[‡,§] Jonathan M. White,[†] Anthony R. White,*[,‡,§] Trevor A. Smith,*[,†,∥] and Paul S. Donnelly*[,†]

[†]School of Chemistry and Bio21 Molecular Science and Biotechnology Institute, [‡]Department of Pathology, and [∥]Ultrafast and Microspectroscopy Laboratories, School of Chemistry, University of Melbourne, Parkville, Melbourne, Victoria 3010, Australia

[§]The Florey Institute of Neuroscience and Mental Health, Parkville, Melbourne, Victoria 3052, Australia

Supporting Information

ABSTRACT: The intracellular distribution of fluorescently labeled copper and zinc bis(thiosemicarbazonato) complexes was investigated in M17 neuroblastoma cells and primary cortical neurons with a view to providing insights into the neuroprotective activity of a copper bis(thiosemicarbazonato) complex known as Cu^{II}(atsm). Time-resolved fluorescence measurements allowed the identification of the Cu^{II} and Zn^{II} complexes as well as the free ligand inside the cells by virtue of the distinct fluorescence lifetime of each species. Confocal fluorescent microscopy of cells treated with the fluorescent copper(II)bis(thiosemicarbazonato) complex revealed significant fluorescence associated with cytoplasmic puncta that were identified to be lysosomes in primary cortical neurons and both lipid droplets and lysosomes in M17 neuroblastoma cells. Fluorescence lifetime imaging microscopy confirmed that the fluorescence signal emanating from the lipid droplets could be attributed to the copper(II) complex but also that some degree of loss of the metal ion led to diffuse cytosolic fluorescence that could be attributed to the metal-free ligand. The accumulation of the copper(II) complex in lipid droplets could be relevant to the neuroprotective activity of Cu^{II}(atsm) in models of amyotrophic lateral sclerosis and Parkinson's disease.

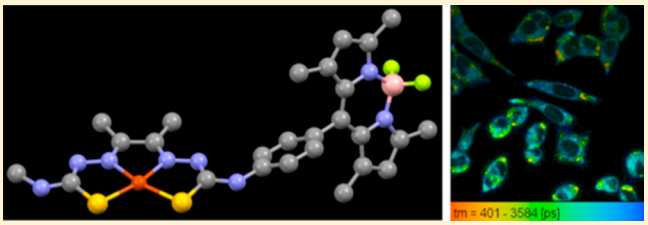

INTRODUCTION

Bis(thiosemicarbazones) have a wide range of pharmacological activity that is linked to their ability to coordinate copper(II) and zinc(II). The resulting complexes are relatively stable, neutral, lipophilic, and often capable of crossing cell membranes. Small modifications to the ligand structure can result in dramatic changes to the chemistry, allowing some degree of control of biological activity. Investigations into the antineoplastic activity of bis(thiosemicarbazones) began in the 1950s when glyoxalbis(thiosemicarbazone) (H_2gtsm) was shown to inhibit sarcoma 180 tumor growth in Swiss mice when administered orally in the diet.[1] It was recognized that chelation of copper and zinc to form either Cu^{II}(gtsm) (Figure 1) or Zn^{II}(gtsm) could be responsible for the antitumor activity.[2]

Sustained interest in the biological activity of metal complexes of bis(thiosemicarbazones) has led to them being used as ligands to coordinate copper radionuclides in diagnostic and therapeutic radiopharmaceuticals.[3−5] A copper complex with two methyl substituents on the backbone of the ligand, Cu^{II}(atsm), where H_2atsm = diacetylbis(4-methyl-3-thiosemicarbazone), is currently in clinical trials as a hypoxia imaging agent,[6−10] whereas the complex with a single methyl substituent on the backbone, Cu^{II}(ptsm), has been investigated as tracer of blood perfusion (Figure 1).[4,11,12]

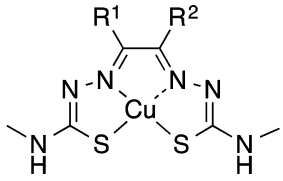

Cu^{II}(gtsm); $R^1 = R^2 = H$
Cu^{II}(ptsm); $R^1 = CH_3$; $R^2 = H$
Cu^{II}(atsm); $R^1 = R^2 = CH_3$

Figure 1. Cu^{II}(gtsm), Cu^{II}(ptsm), and Cu^{II}(atsm).

The presence of two electron-donating methyl groups in Cu^{II}(atsm) stabilizes the Cu^{II} complexes with respect to reduction to Cu^{I}. The Cu^{II}/Cu^{I} reduction potential is $E^{0\prime}$ = −0.59 V for Cu^{II}(atsm), $E^{0\prime}$ = −0.51 V for Cu^{II}(ptsm), and $E^{0\prime}$ = −0.43 V for Cu^{II}(gtsm) (vs Ag/AgCl).[13,14] It is thought that

Received: July 16, 2015
Published: September 23, 2015

DOI: 10.1021/acs.inorgchem.5b01599
Inorg. Chem. 2015, 54, 9556−9567

Scheme 1. Synthesis of H_2L^1, $Cu^{II}L^1$, and $Zn^{II}L^1$

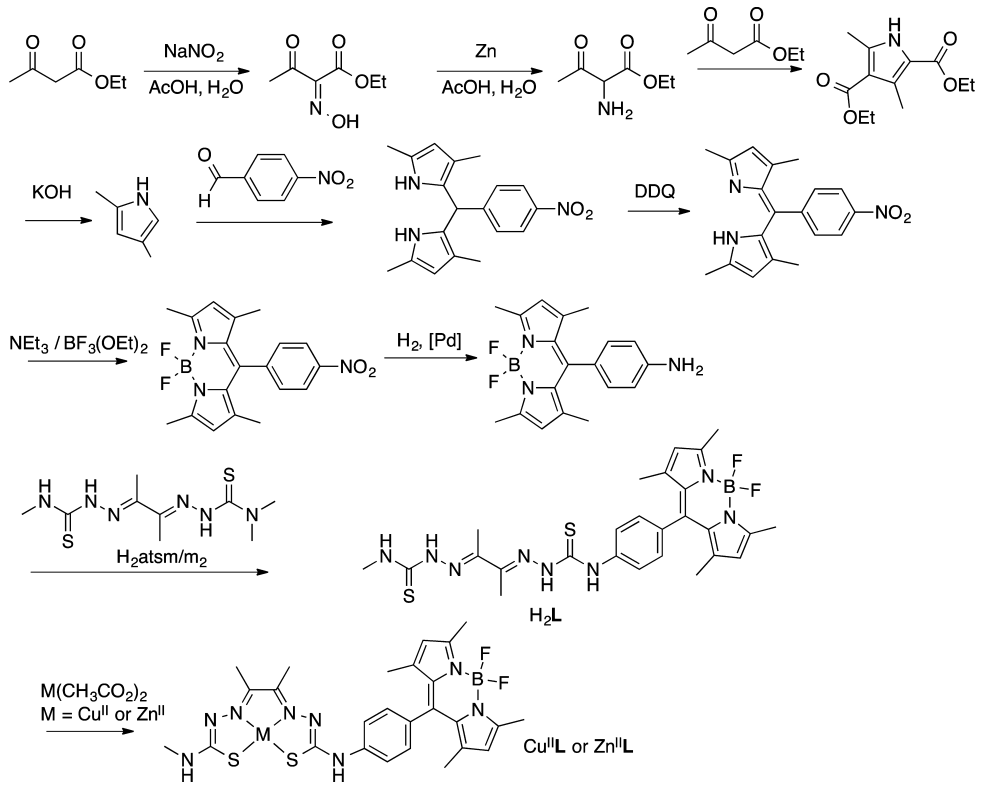

the Cu^{II}/Cu^{I} reduction potential plays an important role in the cellular biology, as the Cu^{II} complexes of bis(thiosemicarbazonato) ligands are stable ($K_A = 10^{18}$) but the Cu^{I} complexes are less stable. It is likely that following intracellular reduction to Cu^{I} the metal ion is susceptible to transfer to copper metallochaperone proteins, consequently becoming increasingly bioavailable.[15]

The intracellular redox-mediated copper-releasing properties of Cu^{II}(gtsm) have been utilized as a unique way to increase intracellular bioavailable copper in cell and animal models of relevance to the pathology of Alzheimer's disease.[16−18] Cu^{II}(atsm) is also of interest as a potential treatment for neurodegeneration, as treatment with Cu^{II}(atsm) resulted in improved motor and cognitive function in four different animal models of Parkinson's disease[19] and improved mouse survival and locomotor function in animal models of amyotrophic lateral sclerosis (ALS).[20−22]

The zinc(II) complexes of bis(thiosemicarbazones), such as Zn^{II}(atsm), are fluorescent, and this intrinsic fluorescence can be used to monitor their cellular uptake and intracellular distribution using fluorescence microscopy.[23−27] The copper(II) complexes of bis(thisoemicarbazones) derived from acenaphthenequinone are weakly fluorescent, and fluorescence microscopy of HeLa cells treated with these complexes revealed significant accumulation in the external cell membrane and relatively slow internalization.[28] Cu^{II}(atsm) is not fluorescent, so to gain insight into the subcellular distribution of Cu^{II}(atsm), a derivative with a fluorescent pyrene functional group was prepared, Cu^{II}(atsm/a-pyrene). This derivative localized in lysosomes in HeLa cancer epithelial cells.[29] The subcellular localization of this complex (Cu^{II}(atsm/a-pyrene)) was also investigated in cells of neuronal origin (M17 neuroblastoma), where the complex accumulated in distinct punctate structures that partially colocalized with lysosomes and an endoplasmic reticulum dye (ER Tracker). There was also some evidence that Cu^{II}(atsm/a-pyrene) associated with autophagic structures.[30] Pyrene-based probes, however, are not ideal for some fluorescence imaging applications, particularly of biological materials, requiring relatively high energy excitation and being susceptible to excimer formation.

Conventional imaging using confocal fluorescence microscopy relies on spatial variation of emission intensity. Most metal complexes with appended fluorophores have similar excitation and emission profiles to the corresponding metal-free ligand. This means that measurement of emission intensity does not discriminate between the intact metal complex and metal-free ligand. This contrasts with cellular imaging using fluorescence lifetime imaging microscopy (FLIM), where emission lifetimes are measured that are normally independent of concentrations (in the absence of aggregation effects), and it is also likely that the emission lifetimes of metal complexes with appended fluorophores will be distinctly different from the emission lifetimes of the metal-free ligands.[31−34] In this Article we describe the use of FLIM to elucidate the subcellular distribution and speciation of a new derivative of H_2atsm tethered to a 4,4-difluoro-4-bora-3a,4a-diaza-*s*-indacene (BODIPY) fluorophore and its copper and zinc complexes. In general BODIPY dyes possess reasonably sharp fluorescence emission and a high fluorescence quantum yield, are reasonably insensitive to pH and solvent polarity, and are sufficiently stable to physiological conditions.[35−37]

During the preparation of this Article independent research was published[38] using an alternative synthetic approach to prepare different BODIPY derivatives of Cu^{II}(atsm) and Cu^{II}(gtsm) where FLIM was used to integrate metal release properties. This work is differentiated from theirs in that the BODIPY fluorophore is linked to the bis(thiosemicarbazone) ligand through an aromatic group rather than a two-carbon

DOI: 10.1021/acs.inorgchem.5b01599
Inorg. Chem. 2015, 54, 9556−9567

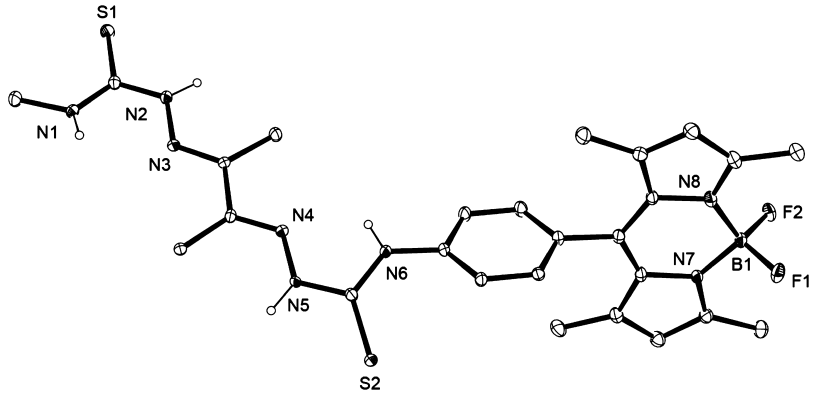

Figure 2. ORTEP (40% probability) representation of H_2**L**. Solvent molecules and selected hydrogen atoms are omitted for clarity.

aliphatic chain but also by extending the study to cells of relevance to models of neurodegeneration with a view to providing some insight into the neuroprotective activity of Cu^{II}(atsm) in mouse models of neurodegenerative diseases.[19−22] In this Article the cellular uptake and intracellular distribution of the new BODIPY-labeled ligand and its copper(II) and zinc(II) complexes was studied in BE(2)-M17 neuroblastoma cells (referred to as "M17" cells henceforth in this Article), a secondary cell line cloned from the SK-N-BE(2) cell line, originating from a metastatic neuroblastoma that has the biochemical properties of neuronal cells when grown in culture.[39] Immortalized secondary cell cultures derived from cancerous cells such as M17 neuronal-like neuroblastoma cells may contain oncogenes or a loss of control of cell replication that can compromise their suitability as models of non-cancerous neurons; so additional studies in murine primary cortical neurons grown in culture were also performed.

RESULTS AND DISCUSSION

Chemical Synthesis. The BODIPY fluorophore was prepared from 2,4-dimethylpyrrole followed by the addition of a *meso*-aryl bridge. The steric hindrance of methyl substituents restricts rotation of the BODIPY core plane (typically at 90°) with respect to the aromatic ring. This electronic decoupling of the π-systems suppresses nonradiative processes, resulting in narrow absorption and emission bands. 2,4-Dimethylpyrrole was prepared according to literature methods by nitrating ethyl acetoacetate with sodium nitrite under acidic conditions, followed by reduction with zinc to produce a primary amine and condensation with a second equivalent of ethyl acetoacetate to give 2,4-dimethyl-3,5-dicarbethoxypyrrole. A global base hydrolysis of the esters gives 2,4-dimethylpyrrole, separated by steam distillation and further purified by fractional distillation (Scheme 1).[40,41]

The atsm-BODIPY ligand, H_2**L**^{1}, was prepared by a high-yielding transamination reaction where a primary amine displaces a tertiary amine on H_2atsm/m_2 (Scheme 1).[42,43] A BODIPY precursor with a primary amine functional group was prepared via condensation of 2,4-dimethylpyrrole with *p*-nitrobenzaldehyde to give a *p*-nitrophenyl-substituted dipyrromethane followed by oxidation with 2,3-dichloro-5,6-dicyano-*p*-benzoquinone (DDQ) and subsequent treatment with $BF_3{\cdot}(OEt)_2$ under basic conditions, which affords 4,4-difluoro-8-(4-nitrophenyl)-1,3,5,7-tetramethyl-4-bora-3a,4a-diaza-*s*-indacene.[44,45] Ligand H_2**L** was prepared in 60% yield, in a two-step, one-pot procedure, by initial reduction of the *p*-nitro functional group to the amine (using H_2, Pd/C) followed by reaction with H_2atsm/m_2 (Scheme 1).

The ^{1}H NMR spectra of H_2**L**^{1} display the expected resonances. The ^{13}C NMR spectrum of H_2**L**^{1} displays all resonances as expected including those for the quaternary thiocarbonyl carbon atoms at δ 178.5 and 176.5 ppm. The ^{19}F NMR spectrum displays a distorted quartet due to ^{19}F−^{11}B coupling (spin = 3/2, 80.1% natural abundance) with a broadened base caused by the overlap of signals associated with ^{19}F−^{10}B coupling (spin = 3, 19.9% natural abundance).

Crystals of H_2**L**^{1} suitable for X-ray crystallography were grown from a saturated solution of H_2**L**^{1} in dimethyl sulfoxide (Figure 2). In the solid state H_2**L**^{1} adopts an (*E*,*E*)-configuration about the imine double bonds and an *s-trans* (antiperiplanar) conformation about the C(3)−C(4) bond similar to H_2atsm.[47] The orthogonal dihedral angle (89.9(9)°) to the plane of the BODIPY demonstrates the restricted rotation of the phenyl group resulting from the steric hindrance between the methyl groups in the 4-position on the pyrrole and the arene ring. The C−S bond lengths of 1.679(4) and 1.670(3) Å indicate, as expected, more thione- than thiol-like character in the "free" ligand.

Orange Zn^{II}**L** and red-brown Cu^{II}**L**^{1} could be prepared by addition of the appropriate metal acetate salt to H_2**L** in acetonitrile or dimethyl sulfoxide (Scheme 1). Alternatively, the Cu complex could be prepared by transmetalation of the Zn complex with the addition of $Cu^{II}(CH_3CO_2)_2$. The ^{1}H NMR spectrum of diamagnetic Zn^{II}**L**^{1} in d_6-dmso is as expected, with coordination of the metal ion and the presence of acetate resulting in double deprotonation of the bis-(thiosemicarbazone) ligand, as suggested by the absence of the expected resonances for the imino thiosemicarbazone protons that are present in the ^{1}H NMR spectrum of the "free" ligand (although it is not possible to rule out an increase in N*H* exchange). Redistribution of electron density throughout the conjugated chelate results in a significant upfield shift of both resonances attributed to the S=C−N*H* protons by 0.5 and 1 ppm and a moderate downfield shift of the bridging aromatic ring resonances by ∼0.25 ppm. The ^{13}C NMR spectrum is of particular interest due to the absence of several expected resonances for quaternary thiocarbonyl and imine carbons. Interestingly, an HMBC experiment identified the imine carbon atoms coupled to the adjacent methyl protons on the bis(thiosemicarbazone) backbone. Both complexes revealed a peak in the ESI mass spectrum corresponding to the expected *m*/*z* value for [M^{II} + H^+] with the expected isotope pattern. An RP-HPLC system coupled with UV/vis detection of Cu^{II}**L**^{1} (t_R

DOI: 10.1021/acs.inorgchem.5b01599
Inorg. Chem. 2015, 54, 9556−9567

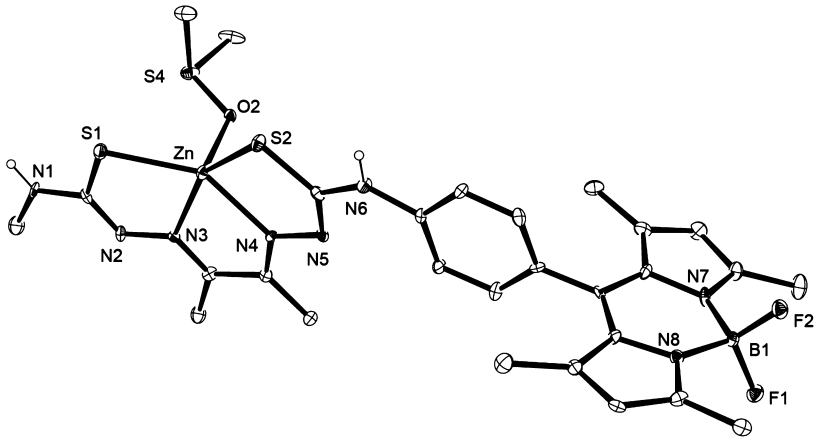

Figure 3. ORTEP (40% probability) representation of $Zn^{II}L^1$. Solvent molecule and selected hydrogen atoms are omitted for clarity.

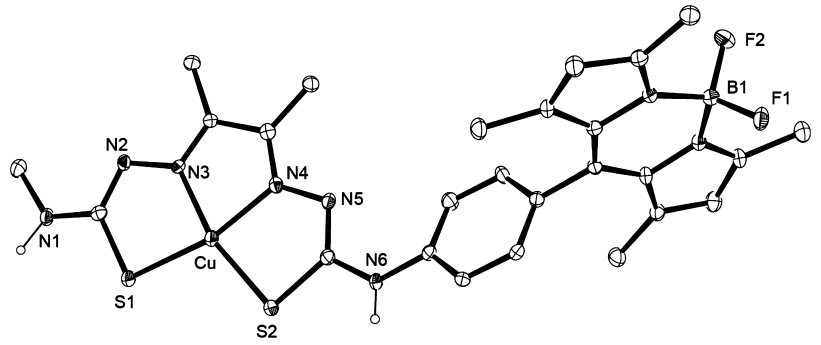

Figure 4. ORTEP (40% probability) representation of $Cu^{II}L^1$. Solvent molecules and selected hydrogen atoms are omitted for clarity.

Table 1. Crystallographic Data for H_2L^1, $Zn^{II}L^1$, and $Cu^{II}L^1$

	H_2L^1	$Zn^{II}L^1$	$Cu^{II}L^1$
chemical formula	$C_{30}H_{43}BF_2N_8O_2S_4$	$C_{30}H_{41}BF_2N_8O_2S_4Zn$	$C_{32}H_{42}BF_2N_{10}O_2S_2Cu$
fw	724.77	788.13	775.23
cryst syst	triclinic	triclinic	triclinic
space group	$P\bar{1}$	$P\bar{1}$	$P\bar{1}$
a/Å	9.6568(10)	11.0973(17)	7.1471(7)
b/Å	10.9113(13)	13.769(3)	15.8888(11)
c/Å	17.452(2)	13.847(2)	17.5263(15)
α/deg	93.022(10)	114.133(17)	66.870(7)
β/deg	105.926(10)	111.069(15)	80.516(8)
γ/deg	90.971(9)	90.039(14)	84.990(7)
V/Å^3	1764.9(3)	1774.6(5)	1804.7(3)
T/K	130(2)	130(2)	130(2)
λ/Å	1.5418 (Cu K/α)	1.5418 (Cu K/α)	1.5418 (Cu K/α)
Z	2	2	2
D_c/g cm^{-3}	1.364	1.475	1.427
abs coeff, μ/mm^{-1}	2.905	3.598	2.404
F(000)	764	820	808
size/mm	0.4 × 0.2 × 0.05	0.10 × 0.06 × 0.01	0.14 × 0.09 × 0.02
$T_{min/max}$	0.85938/1	0.783/0.961	0.791/0.963
$2\theta_{max}$	73.32	67.49	67.49
N_t	11 148	12 139	12 392
N_{ind}	6776	6370	6501
R_{int}	0.0593	0.2313	0.0885
$N_0(I > 2\sigma(I))$	3904	1806	2609
R_1	0.0895	0.2187	0.1332
R_w	0.0475	0.0500	0.0509
GOF on F^2	0.839	0.544	0.683

DOI: 10.1021/acs.inorgchem.5b01599
Inorg. Chem. 2015, 54, 9556−9567

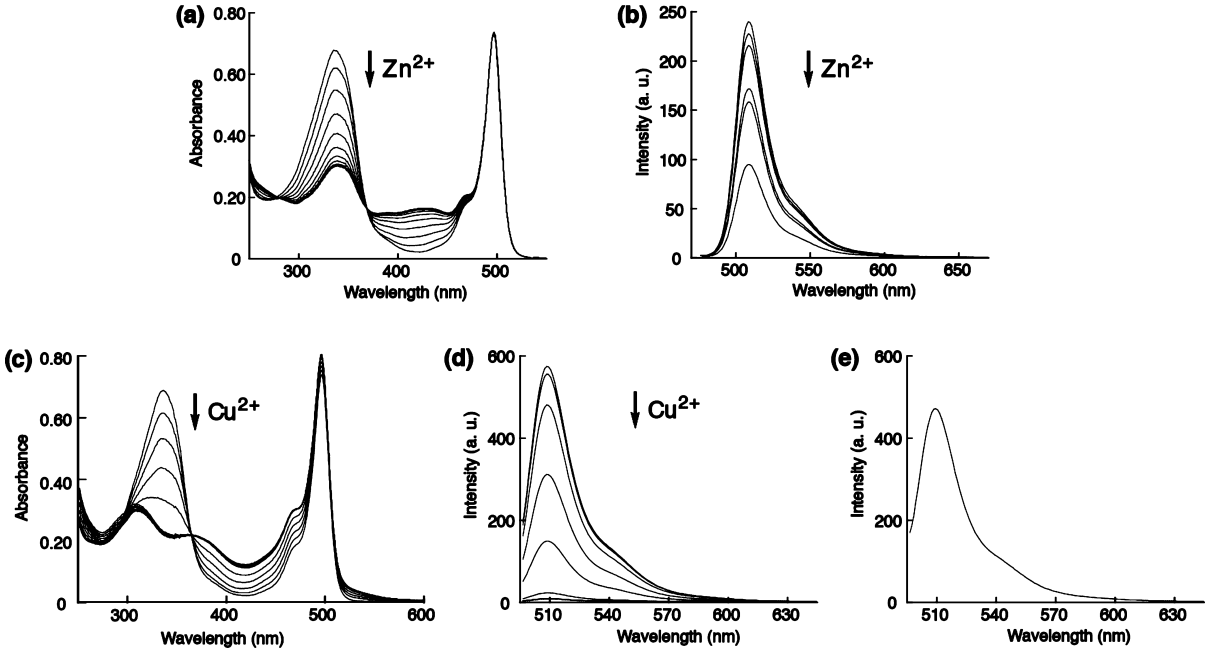

Figure 5. Absorption (a) and fluorescence spectra (λ_{ex} = 490 nm) (b) of $H_2\mathbf{L}^1$ in CH_3CN when titrated with $Zn(NO)_3$ to give $Zn^{II}\mathbf{L}^1$. Absorbance (c) and fluorescence spectra (d) of a solution of $H_2\mathbf{L}^1$ when titrated with $Cu(NO)_3$ to give $Cu^{II}\mathbf{L}^1$, and fluorescence spectrum of $Cu^{II}\mathbf{L}^1$ acquired with an increased applied PMT voltage (e).

= 16.49 min) confirmed the purity of the complex, whereas $Zn^{II}\mathbf{L}^1$ eluted at the same retention as $H_2\mathbf{L}^1$ with the peak giving the same electronic spectrum as the ligand (t_R = 16.08 min) due to instability in the acidic conditions of the mobile phase (0.1% trifluoroacetic acid/acetonitrile/water).

The molecular structure of $Zn^{II}\mathbf{L}^1$ was confirmed by X-ray crystallography (Figure 3). The Zn^{II} is five-coordinate square-pyramidal, with the dianionic tetradentate bis-(thiosemicarbazone) ligand coordinating through two thiolate-like sulfur atoms reflected in the C−S bond lengths of 1.783(7) and 1.740(7) Å compared with 1.679(4) and 1.670(3) Å for $H_2\mathbf{L}^1$ and two azamethinic nitrogen atoms to give a 5−5−5 (*S*, *N*, *N*, *S*) chelate ring system. The Zn^{II} is 0.43(1) Å out of the plane of the bis(thiosemicarbazonato) donor atoms, with the fifth coordination site occupied by oxygen from a molecule of the crystallization solvent, dimethyl sulfoxide. The orientation of the $Zn-N_2S_2$ system is essentially coplanar, with the arene ring is close to perpendicular to the hindered BODIPY fluorophore with a dihedral angle of 80.1(9)°, similar to H21.679(4) and 1.670(3) Å for $H_2\mathbf{L}^1$.

Crystals of $Cu^{II}\mathbf{L}^1$ were grown from a solution of $Cu^{II}\mathbf{L}^1$ in dimethylformamide. A representation of the molecular structure of $Cu^{II}\mathbf{L}^1$ (Figure 4) reveals the copper binding to the tetradentate ligand in a similar manner to $Zn^{II}\mathbf{L}^1$, but the copper(II) is in a four-coordinate distorted square planar geometry. As seen for $Zn^{II}\mathbf{L}^1$, coordination results in two thiolate-like sulfur atom C−S bond lengths of 1.764(5) and 1.769(5) Å, which are similar to the C−S bond distances in Cu^{II}(atsm), as are the Cu−N and Cu−S bond lengths.[46,47]

Electronic Spectroscopy. The absorption and emission spectroscopic properties of $H_2\mathbf{L}^1$ in an acetonitrile solution were evaluated, and two absorption bands are prominent: the first at λ = 337 nm is attributed to the bis(thiosemicarbazone) fragment ($\varepsilon = 6.7 \times 10^4$ cm^{-1} M^{-1}), and the second at λ = 497 nm ($\varepsilon = 7.3 \times 10^4$ cm^{-1} M^{-1}), with a shoulder at λ = 480 nm ($\varepsilon = 2.0 \times 10^4$ M), is attributed to the BODIPY fluorophore (Figure 5a). The ligand is fluorescent (ϕ_f = 0.29) with an emission peak at λ_{em} = 510 nm (λ_{ex} = 490 nm) with a sharp profile and small Stokes shift characteristic of a BODIPY fluorophore (Figure 5b).

Upon titration of $H_2\mathbf{L}^1$ with Zn^{2+}, the intensity of the ligand-based bis(thiosemicarbazone) absorbance collapses ($\varepsilon = 3.0 \times 10^4$ cm^{-1} M^{-1}) and evidence of a broad absorption at 420 nm ($\varepsilon = 1.6 \times 10^4$ cm^{-1} M^{-1}), characteristic of a bis-(thiosemicarbazonato)Zn^{II} MLCT band, appears. This is accompanied by two isosbestic points, at λ = 279 nm and λ = 369 nm. Addition of Zn^{2+} results in a decrease in the fluorescence intensity by ca. 2.5-fold (Figure 5b) to give a fluorescence quantum yield of ϕ_f = 0.01 for $Zn^{II}\mathbf{L}^1$.

Titration of Cu^{2+} into a solution of $H_2\mathbf{L}^1$ resulted in a collapse in the absorbance attributed to the bis-(thiosemicarbazone) fragment and a hypsochromic shift to 309 nm ($\varepsilon = 3.2 \times 10^4$ cm^{-1} M^{-1}) (Figure 5c). A broad absorption centered at λ = 365 nm ($\varepsilon = 2.2 \times 10^4$ cm^{-1} M^{-1}) is characteristic of MLCT behavior. The copper complex is still fluorescent, λ_{em} = 510 nm (λ_{ex} = 490 nm), but a significant quenching of fluorescence is observed (Figure 5d). The comparatively strong fluorescence of $H_2\mathbf{L}^1$ allows the use of a low photomultiplier voltage on the spectrometer, but the weak fluorescence of $Cu^{II}\mathbf{L}^1$ (ϕ_f = 0.005) is best observed by using a higher voltage gain (Figure 5e).

Electrochemistry. The electrochemistry of $H_2\mathbf{L}^1$, $Zn^{II}\mathbf{L}^1$, and $Cu^{II}\mathbf{L}^1$ was investigated by cyclic voltammetry in dimethylformamide, with a glassy carbon working electrode against a Ag^+/Ag reference electrode (potentials are quoted versus an internal ferrocinium/ferrocene couple where $E^{0\prime}_{1/2}$(Fc/Fc$^+$) = 0.54 V vs SCE; $E^{0\prime}_{1/2}$ = midpoint between a reversible reductive (E_{pc}) and oxidative (E_{pa}) couple, so $E^{0\prime}_{1/2} = (E_{pc} + E_{pa})/2$). All compounds exhibit a one-electron quasi-reversible process between −1.05 and −1.20 V that can be attributed to the reduction of the BODIPY fragment to the radical anion (BODIPY$^{\bullet-}$).[36] The quasi-reversible process at

DOI: 10.1021/acs.inorgchem.5b01599
Inorg. Chem. 2015, 54, 9556−9567

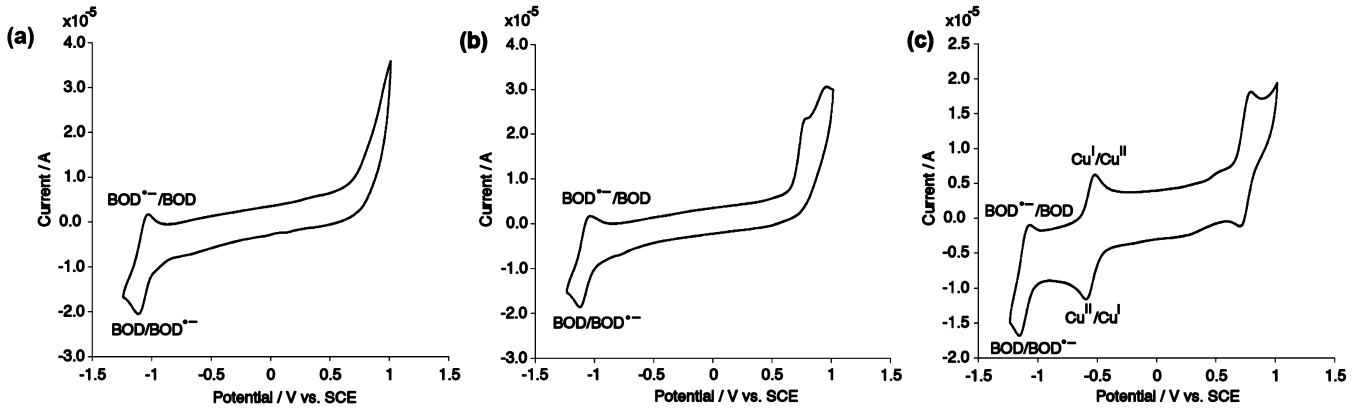

Figure 6. Cyclic voltammograms (scan rate = 100 mV s^{-1}) for 0.1 mM solutions of compounds of (a) $H_2\mathbf{L}^1$, (b) $Zn^{II}\mathbf{L}^1$, and (c) $Cu^{II}\mathbf{L}^1$ in dimethylformamide (10 mM tetrabutylammonium tetrafluoroborate). Potentials are quoted relative to ferrocene ($E_m(Fc/Fc^+)$ = 0.54 V).

$E^{0\prime}{}_{1/2}$ = −0.6 V is attributed to the $Cu^{II/I}$ process and is at a similar potential to Cu^{II}(atsm) that occurs at $E^{0\prime}{}_{1/2}$ = −0.62 V under the same conditions (Figure 6).[13−15] This is important given the correlations between $Cu^{II/I}$ reduction potentials and the biological activity of copper complexes of bis(thiosemicarbazones). Oxidative processes close to E = 0.75 V and E = 0.90 V in $Zn^{II}\mathbf{L}^1$ and $Cu^{II}\mathbf{L}^1$, respectively, are possibly due to the formation of the BODIPY radical cation ($BODIPY^{\bullet+}$),[36] which overlaps with another oxidation process in the case of $Cu^{II}\mathbf{L}^1$ that is due to either a $Cu^{III/II}$ process or oxidation associated with a ligand-based orbital with π-character (the analogous oxidative process in Cu^{II}(atsm) occurs at $E^{0\prime}{}_{1/2}$ = 0.69 V).[48,49]

Cellular Uptake of Complexes and Colocalization. Treatment of both primary cortical neurons and M17 neuroblastoma cells with $Cu^{II}\mathbf{L}^1$ (25 μM) at 37 °C was monitored by live cell scanning confocal fluorescence microscopy and transmitted light/bright field imaging. There was no evidence of changes to cell morphology after incubation for several hours with respect to the control, suggesting that the complex did not cause observable cell death or any other visual cell stress. This behavior is consistent with treatments with comparable concentrations with Cu^{II}(atsm). The fluorescence from $Cu^{II}\mathbf{L}^1$ is distributed throughout the cytosol in live cell M17 neuroblastoma, but significant puncta with high fluorescence intensity are also present (Figure 7). Colocalization studies with Lysotracker showed that some of the punctate regions of high fluorescence intensity associated with $Cu^{II}\mathbf{L}^1$ are within lysosomes (Figure 7d and e). Most of the bright punctate staining is colocalized with HCS lipidTOX neutral deep red lipid stain (shown in blue, Figure 7c), and these punctate regions could also be visualized through transmitted light or bright field imaging, with features characteristic of neutral lipid droplets.[50−53] In cell culture, various amounts of neutral lipids are known to accumulate in lysosomes, and it has been shown that basal levels of lipids are found within lysosomes in neurons.[54,55]

Investigation of primary cortical neurons revealed apparent colocalization between Lysotracker and the neutral lipid stain, with a majority of lysosomes in our primary cortical neuron culture also staining positive for neutral lipids (Figure 8). These punctate regions, positive for Lysotracker and neutral lipid stain, also accumulated $Cu^{II}\mathbf{L}^1$ (Figures 8b−e). As with the M17 cells, $Cu^{II}\mathbf{L}^1$ is absent from the cell nucleus, resulting in a diffuse cytosolic distribution but also distinct bright puncta. In the primary cortical neurons, all punctate regions were found to stain positive for Lysotracker (shown in red) (Figure 8c). These lysosomes also stained positive for the neutral lipid stain (blue, Figure 8d), and together with the green BODIPY fluorophore from $Cu^{II}\mathbf{L}^1$, the overlay of the three primary colors shows as overall white puncta (Figure 8e).

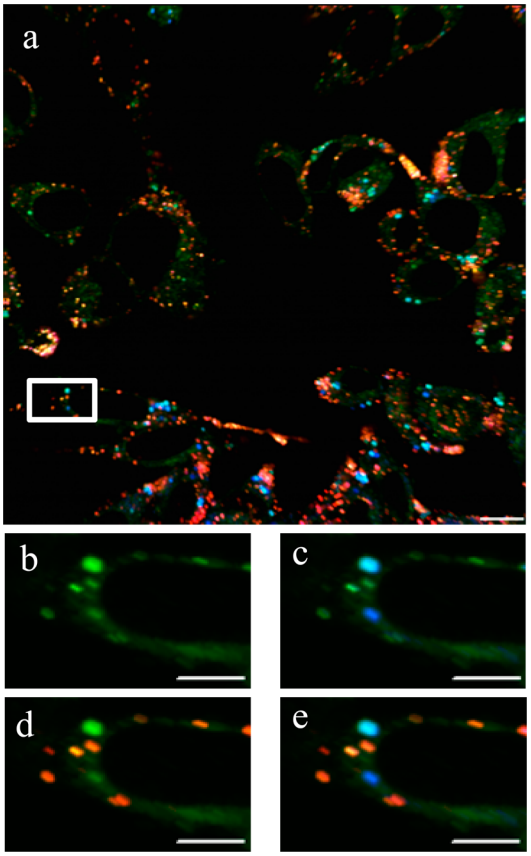

Figure 7. (a) Live cell confocal image of M17 cells treated with $Cu^{II}\mathbf{L}^1$ (green, λ_{ex} = 488 nm), Lysotracker (red, λ_{ex} = 568 nm), and neutral lipid stain (blue, λ_{ex} = 640 nm). Scale bar = 10 μm. (b) Magnified section (indicated by a white box in part a) showing $Cu^{II}\mathbf{L}^1$. (c) $Cu^{II}\mathbf{L}^1$ overlay with neutral lipid stain, showing partial colocalization with $Cu^{II}\mathbf{L}^1$ and lipid droplets. (d) $Cu^{II}\mathbf{L}^1$ overlay with Lysotracker, showing partial colocalization with $Cu^{II}\mathbf{L}^1$ and lysosomes. (e) Overlay of $Cu^{II}\mathbf{L}^1$ (green), Lysotracker (red), and neutral lipid stain (blue). Scale bar = 3 μm.

DOI: 10.1021/acs.inorgchem.5b01599
Inorg. Chem. 2015, 54, 9556−9567

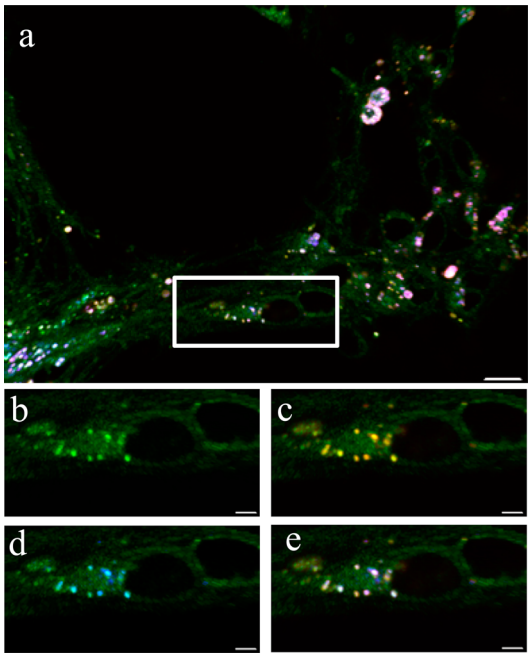

Figure 8. (a) Live cell confocal image of primary cortical neurons, isolated from E14 mice, treated with $Cu^{II}L^1$ (green, λ_{ex} = 488 nm), Lysotracker (red, λ_{ex} = 568 nm), and neutral lipid stain (blue, λ_{ex} = 640 nm). Scale bar = 10 μm. (b) Magnified section indicated by a white box in part a showing $Cu^{II}L^1$. (c) $Cu^{II}L^1$ overlay with Lysotracker, showing partial colocalization with $Cu^{II}L^1$ and lysosomes. (d) $Cu^{II}L^1$ overlay with neutral lipid stain, showing partial colocalization with $Cu^{II}L^1$ and lipid droplets. (e) Overlay of $Cu^{II}L^1$ (green), Lysotracker (red), and neutral lipid stain (blue). Scale bar = 3 μm.

Time-Resolved Fluorescence. Fluorescence lifetime imaging can provide valuable information complementary to that obtained using conventional confocal fluorescence intensity-based imaging particularly relating to the molecular nature of the fluorescent species. The free ligand H_2L^1, $Cu^{II}L^1$, and $Zn^{II}L^1$ emit at similar wavelengths ($\lambda_{em} \approx 510$ nm) (Figure 5) despite their differences in quantum yield, so it is not possible to distinguish between them inside cells by confocal microscopy. However, both the Zn^{II} and Cu^{II} complexes have dramatically different fluorescence lifetimes when compared to the free ligand. Time-resolved emission measurements were carried out, using time-correlated single-photon counting, on the ligand and the complexes in bulk solution in order to characterize their fluorescence lifetimes (Figure S1, Supporting Information). The ligand H_2L^1 displays a fluorescence decay profile adequately fitted by a single-exponential decay function, giving a fluorescence lifetime of 2.83 ns. In comparison, fitting the fluorescence decay curves of the Zn and Cu complexes requires double-exponential decay functions. $Cu^{II}L^1$ has a signature dominant (76%) initial short decay component of $\tau_1 \approx 250$ ps along with a relatively minor contribution from a longer lived decay component of $\tau_2 \approx 2.79$ ns. Similarly, $Zn^{II}L^1$ has a dominant (83%) short decay component of ~170 ps and a minor (17%) long decay component of $\tau_2 \approx 2.55$ ns. These findings are in general agreement with those of Dilworth et al. on related but structurally different bis(thiosemicarbazone) complexes conjugated to a BODPY fluorophore through a two-carbon aliphatic linker except that for the complexes presented here, $Zn^{II}L^1$ and $Cu^{II}L^1$, the longer lifetime component does not exceed that of the free ligand.[38] The dominant short decay component of the fluorescence of both complexes is attributed to the quenched emission of the ligand, as its magnitude relative to the free ligand correlates well with the degree of

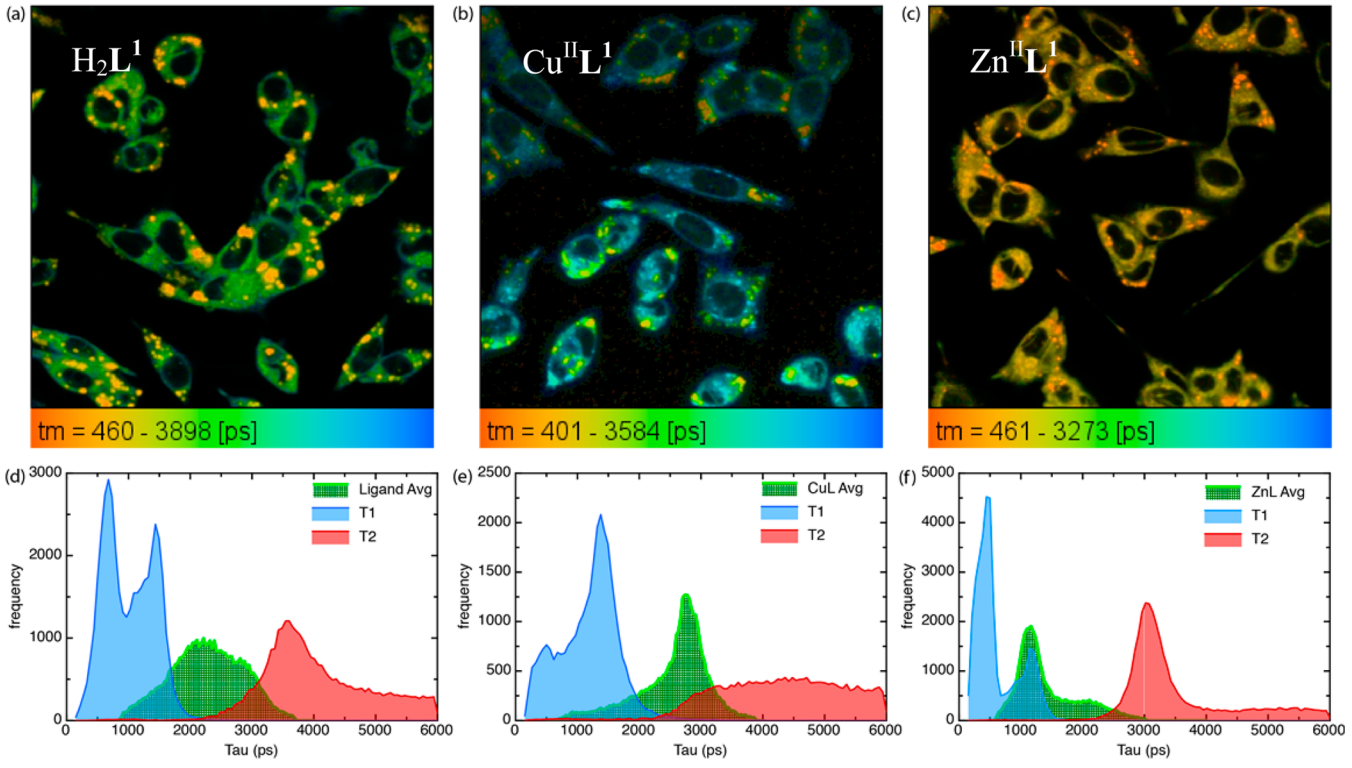

Figure 9. Fluorescence lifetime images with color scales mapping the mean fluorescence lifetime for (a) H_2L, (b) $Cu^{II}L^1$, and (c) $Zn^{II}L^1$, respectively, in M17 cells. (d, e, and f) Corresponding fluorescence lifetime distributions/histograms for the average fluorescence lifetime, τ_{av}, τ_1, and τ_2.

DOI: 10.1021/acs.inorgchem.5b01599
Inorg. Chem. 2015, 54, 9556−9567

quenching of fluorescence observed in steady-state spectra when the coordination complex is formed. The similarity of the long decay times of the complexes to that of the free ligand's single decay process suggests that this component can be broadly attributed to residual unquenched ligand-based processes.

Fluorescence Lifetime Imaging Microscopy. Fluorescence lifetime imaging microscopy was performed on M17 cells separately incubated with $H_2\mathbf{L}^1$, $Cu^{II}\mathbf{L}^1$, or $Zn^{II}\mathbf{L}^1$, with the corresponding emission intensity and lifetime maps shown in Figure 9a–c, respectively. The experimental acquisition times required for the FLIM images of the cells containing the metal complexes were substantially longer than in the case where just the ligand was present due to the quenching induced by the metal ion. The images shown represent fluorescence lifetime maps resulting from double-exponential fitting in each pixel across the entire image, with the color indicative of the amplitude-weighted mean fluorescence lifetime, τ_{av}, in each pixel (see color legend). This is in contrast with conventional confocal images, in which emission *intensity* is plotted, which can be influenced by fluorophore concentration and environment/speciation. We do not associate the discrete fluorescence lifetimes with two specific emitting species, but an interpretation of the double-exponential analysis used to generate the FLIM images is still informative.

Along with each FLIM image is shown the corresponding lifetime distribution plots for the average fluorescence lifetime, τ_{av} (red traces), and the two individual lifetime components, τ_1 and τ_2, recovered from the biexponential analysis of the fluorescence lifetime images of $H_2\mathbf{L}^1$, $Cu^{II}\mathbf{L}^1$, and $Zn^{II}\mathbf{L}^1$ (Figure 9d–f, respectively). The distribution of fluorescence lifetimes throughout the M17 cells incubated with the complexes displays the same diffuse cytosolic distribution characteristic of partial lysosomal/partial lipid droplet localization, as shown using live cell confocal imaging with Lysotracker and a neutral lipid stain (Figure 7), and these punctate regions show a higher propensity for the short-lived copper and zinc complexes, shown as yellow/orange puncta inside the cells (Figure 9). The diffuse cytosolic fluorescence tends to be due to emission with a longer lifetime, shown as diffuse blue/green regions within the cytosol (Figure 9). As with the confocal images (Figure 7) there is no detectable fluorescence within the cell nucleus (Figure 9).

Treatment of the cells with $H_2\mathbf{L}^1$ (Figure 9a) shows a broad average lifetime distribution with components that exhibit both shorter and longer fluorescence lifetimes (Figure 9d) compared with that characteristic of $H_2\mathbf{L}^1$ in solution reported above (~2.83 ns). There is some evidence of a slight shoulder on the distribution at around this lifetime. The broadness of this distribution most likely reflects a wide range of local environments experienced by $H_2\mathbf{L}^1$, in agreement with the findings of Dilworth et al.[38] The distribution toward short-lived decay components is presumably representative of the emission of the ligand being quenched to some degree probably due to the presence of trace copper and zinc in cell media and cells leading to the formation of copper or zinc complexes of $\mathbf{L}^1$. The longer-lived components of the distribution may correspond to an enhanced emission quantum yield due to a slightly more rigid environment experienced by the fluorophore or may be indicative of some degree of metabolic cleavage of the BODIPY fragment from the rest of the ligand, as dyes of this family typically have fluorescence lifetimes of several (up to 5) nanoseconds.

Treatment of cells with $Cu^{II}\mathbf{L}^1$ results in images with significantly different behavior compared to cells treated with $H_2\mathbf{L}^1$; the τ_{av} distribution is far narrower and is dominated by emission with a lifetime characteristic of the free ligand (~2.8 ns). This suggests that the $Cu^{II}\mathbf{L}^1$ experiences a more uniform range of cellular environments than $H_2\mathbf{L}^1$ alone and perhaps that a proportion of the copper(II) is being released from the complex upon incubation with the cells. Treatment of M17 cells with $Zn^{II}\mathbf{L}^1$ results in images where the lifetime distribution is, somewhat surprisingly, dominated by a narrow peak centered at around 1.4 ns, which is not apparent for $Zn^{II}\mathbf{L}^1$ in solution. A broad shoulder on the distribution is apparent at around the lifetime reported above for this complex in solution (2–2.5 ns), again suggesting that a proportion of the Zn is being lost from the complex during incubation.

For $H_2\mathbf{L}^1$ alone (Figure 9d) the τ_{av} distribution indicates that any association with metal ions taken up from the cellular environment must be minimal, as the measurements in bulk solution show that the emission is quenched significantly ($\tau_f \approx$ 200 ps) when the ligand is fully complexed with Cu or Zn, whereas the τ_{av} distribution does not indicate any subnanosecond lifetime components. However, the τ_{av} distributions are somewhat misleading, being weighted toward the longer lived components by the generally minor contribution (in terms of the pre-exponential factors of the biexponential analysis) of very broad τ_2 distributions, generally maximized at ~3–4 ns, that again might indicate some loss of the fluorophore from the ligand.

The most information is gained by concentrating on just the shorter lived (τ_1) components in the fluorescence lifetime distributions (blue traces in Figure 9d–f). Two peaks are apparent at ~1400 and ~500 ps in the distributions of all three molecules, and the relative abundance of these distribution bands is dependent on the complex. The peak at ~1400 ps dominates the τ_1 distribution in the case of $Cu^{II}\mathbf{L}^1$ (Figure 9e) but is the minor feature in the $Zn^{II}\mathbf{L}^1$ case (Figure 9f), which is instead dominated by the shorter lifetime contribution (~500 ps). In the case where the cells have been treated with $H_2\mathbf{L}^1$ (Figure 9d), the 1400 and ~500 ps components are roughly equivalent in their contribution. This short-lived ($\tau_1 \leq 550$ ps) emission is a characteristic of $Cu^{II}\mathbf{L}^1$ and $Zn^{II}\mathbf{L}^1$, so the peaks at around 500 and 1400 ps are likely to be a consequence of the free ligand, as expected, coordinating to Cu^{II}/Zn^{II} in the cell media or intracellular environment.

For the cells treated with $Cu^{II}\mathbf{L}^1$ the τ_1 distribution has a larger peak around 1400 ps due to the presence of $Cu^{II}\mathbf{L}^1$, but there is also evidence of a peak at around 500 ps consistent with the presence of $Zn^{II}\mathbf{L}^1$, suggesting that, at least to some degree, $Cu^{II}\mathbf{L}^1$ is releasing copper, most likely through reduction of the metal to Cu^{I}, which is then sequestered by intracellular copper-binding proteins, and the liberated ligand is now capable of binding to zinc, leading to the formation of $Zn^{II}\mathbf{L}^1$. Intracellular zinc concentrations are higher than intracellular copper concentrations, and Cu^{I} is largely bound to high-affinity chaperone proteins.[15]

The τ_1 component for the $Zn^{II}\mathbf{L}^1$-treated cells shows a large peak around 500 ps, with a smaller peak around 1400 ps, once again consistent with metal exchange and that the $Zn^{II}\mathbf{L}^1$ complex zinc can be transmetalated to give $Cu^{II}\mathbf{L}^1$. The rapid exchange of Zn^{II} for Cu^{II} in bis(thiosemicarbazone) complexes has been used in radiolabel bis(thiosemicarbazones) with radioactive copper isotopes[48,56] and has been shown to occur in cell culture[16] and *in vivo* in a SOD1G37R mouse model of

DOI: 10.1021/acs.inorgchem.5b01599
Inorg. Chem. 2015, 54, 9556–9567

familial ALS.[22] The formation of copper(II) bis-(thiosemicarbazonato) complexes by transmetalation of their Zn^{II} complexes has also been implicated in their antitumor activity.[57]

$Cu^{II}L^1$ Accumulates in Lipid Droplets. The FLIM measurements reveal that the strong fluorescence observed in the large puncta in cells treated with $Cu^{II}L^1$ are due to the copper complex (Figure 9b). These puncta appear to be lipid droplets based on their colocalization with HCS lipidTOX neutral deep red lipid stain (Figure 7). Lipid droplets are "cytoplasmic lipid inclusions consisting of a core of neutral lipids such as triacylglycerols and cholesteryl esters surrounded by a monolayer of phospholipids and associated proteins".[50] The lipids stored in lipid droplets are used for metabolism, membrane synthesis, and steroid synthesis. Lipid droplets are thought to play a fundamental role in intracellular lipid homeostasis and in storing cholesterol in the form of cholesterol esters. Assuming that the subcellular localization of this fluorescently labeled derivative of Cu^{II}(atsm) reflects the cellular distribution of the parent compound, the accumulation of $Cu^{II}L^1$ within lipid droplets is of potential interest to the neuroprotective activity of Cu^{II}(atsm) in models of ALS and Parkinson's disease. Mitochondrial defects in neurons lead to elevated levels of reactive oxygen species that can elevate lipid synthesis in neurons and result in the formation of lipid droplets in glial cells. It is also worth noting that impaired mitochondrial electron transfer leads to increased cellular retention of copper in cells treated with Cu^{II}(atsm).[58,59] The lipid droplets in glia contribute to neurodegeneration through elevated levels of lipid peroxidation. In *Drosophila* and mice lipid droplets form in glia before or at the onset of degeneration, and disruption to lipid droplet metabolism can contribute to neurodegeneration.[60] The formation and metabolism of lipid droplets have also been identified as playing a role in a subtype of ALS caused by mutations in human VAMP (vesicle-associated membrane protein).[61] The Cu^{II}(atsm) complex possesses both a reductive $Cu^{II/I}$ couple and an oxidative process that has been attributed to either oxidation of the metal ($Cu^{III/II}$) or ligand-based electrochemistry. The accumulation of redox-active Cu^{II}(atsm) in lipid droplets could partially explain the fact that treatment with Cu^{II}(atsm) resulted in lower levels of lipid peroxidation in a model of ischemic reperfusion injury[62] and could also lead to less peroxidation of lipids in glia partially contributing to the neuroprotective activity of the complex in mouse models of ALS.[20] It is also possible that the presence of Cu^{II}(atsm) in lipid droplets could protect these vital lipids from peroxynitrite ($ONOO^-$)-mediated nitration, but further studies are required to substantiate such speculation.[19] Radiolabeled Cu^{II}(atsm) is currently under evaluation as a hypoxia tracer, and lipid droplets become an important source of energy for cell proliferation and may serve a protective role in hypoxic environments. Therefore, it is interesting to speculate that changes to lipid droplet metabolism could contribute to increased accumulation of Cu^{II}(atsm) in hypoxic cells.[60]

Concluding Remarks. A new fluorescent derivative of H_2atsm tethered to a BODIPY fluorophore (H_2L^1) has been prepared using a transamination reaction where a primary amine on a BODIPY fluorophore displaces a tertiary amine on H_2atsm/m_2. The ligand and its neutral Cu^{II} and Zn^{II} complexes have been characterized by X-ray crystallography and reveal that addition of the fluorescent tag does not change the coordination environment of the metal ion when compared to the parent complexes, Cu^{II}(atsm) and Zn^{II}(atsm). The biological activity of Cu^{II}(atsm) is at least partially dependent on the $Cu^{II/I}$ reduction potential, and electrochemical measurements using cyclic voltammetry revealed that $Cu^{II}L^1$ possesses a quasi-reversible reduction at a similar potential to Cu^{II}(atsm). Ligand H_2L^1 is fluorescent with a narrow emission band characteristic of BODIPY (λ_{em} = 510 nm, λ_{ex} = 490 nm, ϕ_f = 0.29). Coordination of either Zn^{II} or Cu^{II} to the ligand results in a significant quenching of fluorescence, but both $Zn^{II}L^1$ and $Cu^{II}L^1$ are still fluorescent. The free ligand H_2L^1, $Cu^{II}L^1$, and $Zn^{II}L^1$ all emit at similar wavelengths ($\lambda_{em} \approx$ 510 nm), so it is not possible to distinguish between them inside cells by conventional confocal microscopy. However, $Zn^{II}L^1$ and $Cu^{II}L^1$ have shorter fluorescence lifetimes than the free ligand H_2L^1, so FLIM enables important information on the nature of the emitting species visible with fluorescent microscopy.

Confocal microscopy of neuronal cells treated with $Cu^{II}L^1$ revealed significant fluorescence signal associated with distinct cytosolic puncta, which were found to be lysosomes that also stained positive for lipid in primary cortical neurons or a combination of lysosomes and lipid droplets in secondary M17 neuroblastoma cells. FLIM measurements were able to identify that treatment of cells with $Cu^{II}L^1$ led to the complex accumulating in large cytoplasmic inclusions that were consistent with the lipid droplets identified by confocal microscopy but also, at least to some extent, release of the metal ion to give H_2L^1 and $Zn^{II}L^1$ presumably due to the liberated ligand coordinating to bioavailable zinc. Treatment with $Zn^{II}L^1$ also resulted in the accumulation of the zinc complex in cytoplasmic inclusions but also some degree of transmetalation to form the copper complex. This work adds to the growing examples where FLIM has provided valuable complementary information to conventional confocal fluorescent microscopy.[31−34,38] It would be of interest to apply FLIM to the characterization of sensors designed to probe the cellular metabolism of copper as a complementary approach to ratiometric fluorescent probes.[63−66] The biological activity of Cu^{II}(atsm) can be related to the stability of the complex and its $Cu^{II/I}$ reduction potential, and in these respects the fluorescent derivative, $Cu^{II}L^1$, retains these properties. However, it is acknowledged that the addition of the BODIPY fluorophore could result in a copper complex with a different intracellular distribution from the parent compound. Providing the intracellular distribution of $Cu^{II}L^1$ accurately reflects the behavior of Cu^{II}(atsm), the colocalization within lipid droplets could be relevant to the neuroprotective activity of Cu^{II}(atsm), as disruption to lipid droplet metabolism has been identified as contributing to neurodegeneration. These results also suggest it is of interest to investigate the significance of the oxidative redox couple displayed by Cu^{II}(atsm) to its biological activity. Further studies that probe the interplay between treatment of cells with Cu^{II}(atsm), lipid droplet metabolism, and neuroprotection are warranted.

EXPERIMENTAL SECTION

Crystallography. Crystals of H_2L^1, $Zn^{II}L^1$, and $Cu^{II}L^1$, respectively, were mounted in low-temperature oil, then flash cooled to 130 K using an Oxford low-temperature device. Intensity data were collected at 130 K with an Oxford XCalibur X-ray diffractometer with a Sapphire CCD detector using Cu Kα radiation (graphite crystal monochromator, λ = 1.541 84 Å). Data were reduced and corrected for absorption.The structures were solved by direct methods and difference Fourier synthesis using the SHELX suite of programs as implemented within the WINGX software.[67,68] Thermal ellipsoid plots

DOI: 10.1021/acs.inorgchem.5b01599
Inorg. Chem. 2015, 54, 9556−9567

were generated using the program ORTEP-3 integrated within the WINGX suite of programs.[68] CCDC deposition numbers: 1402571, 1402572, and 1402573.

General Procedures. All reagents and solvents were obtained from commercial sources (Sigma-Aldrich) and used as received unless otherwise stated. 2,4-Dimethylpyrrole,[40,41] diacetyl-4-methyl-4′-dimethyl-3-bis(thiosemicarbazone) (atsmm$_2$),[42] 4,4-difluoro-8-(4-nitrophenyl)-1,3,5,7-tetramethyl-4-bora-3a,4a-diaza-*s*-indacene (*p*-NO$_2$BODIPY), and 8-(4-aminophenyl)-4,4-difluoro-1,3,5,7-tetramethyl-4-bora-3a,4a-diaza-*s*-indacene (*p*-NH$_2$BODIPY)[44,45] were prepared following published procedures. Elemental analyses for C, H, and N were carried out by Chemical & MicroAnalytical Services Pty. Ltd., Vic. Nuclear magnetic resonance spectra were recorded on a Varian FT-NMR 500 spectrometer (^{1}H NMR at 499.9 MHz, ^{13}C NMR at 125.7 MHz, and ^{19}F NMR at 471 MHz) at 298 K and referenced to the internal solvent residue for ^{1}H and ^{13}C and external hexafluorobenzene (δ −164.9 ppm) for ^{19}F. Mass spectra were recorded on an Agilent 6510-Q-TOF LC/MS mass spectrometer and calibrated to internal references.

UV/Visible Spectroscopy. UV/vis spectra were recorded on a Cary 300 Bio UV−vis spectrophotometer, from 800 to 200 at 0.5 nm data intervals with a 600 nm/min scan rate. Solutions of H$_2$**L**^{1} in acetonitrile (10 μM) were titrated with 6 μL aliquots of standardized Cu(NO$_3$)$_2$ or Zn(NO$_3$)$_2$ solutions (1 mM in H$_2$O). Successive scans were performed measuring absorbance every 2 min (800−250 nm).

Fluorescence Spectroscopy. Fluorescence emission spectra were measured on a Varian Cary Eclipse fluorescence spectrophotometer. Solutions of H$_2$**L**^{1} in acetonitrile (300 nM) were titrated with 2 μL aliquots of standardized Cu(NO$_3$)$_2$ or Zn(NO$_3$)$_2$ solutions (1 mM in H$_2$O). Successive scans were performed measuring fluorescence (λ_{ex} = 490 nm) emission between 510 and 700 nm.

High-Performance Liquid Chromatography. Analytical RP-HPLC traces were acquired using an Agilent 1200 series HPLC system equipped with an Agilent Zorbax Eclipse XDB-C18 column (4.6 × 150 mm, 5 mm) with a 1 mL/min flow rate and UV spectroscopic detection at 214, 220, and 270 nm. Retention times (t_R/min) were recorded using a gradient elution method of 0−100% B over 25 min; solution A consisted of water (buffered with 0.1% trifluoroacetic acid), and solution B consisted of acetonitrile (buffered with 0.1% trifluoroacetic acid).

Electrochemistry. Cyclic voltammograms were recorded using an AUTOLAB PGSTAT100 equipped with GPES V4.9 software. Measurements of the complexes were carried out at approximately 1 × 10^{-4} M in dimethylformamide with tetrabutylammonium tetrafluoroborate (1 × 10^{-2} M) as electrolyte using a glassy carbon disk (*d*, 3 mm) working electrode, a Pt wire counter/auxiliary electrode, and a Ag/Ag$^+$ pseudo reference electrode (silver wire in H$_2$O (KCl (0.1 M)/AgNO$_3$ (0.01 M))). Ferrocene was used as an internal reference (E_m(Fc/Fc$^+$) = 0.54 V vs SCE), where E_m refers to the midpoint between a reversible reductive (E_{pc}) and oxidative (E_{pa}) couple, given by $E_m = (E_{pc} + E_{pa})/2$. Irreversible systems are given only reductive (E_{pc}) and oxidative (E_{pa}) values, respectively.

Diacetyl-4-methyl-4′-(8-(4-aminophenyl)-4,4-difluoro-1,3,5,7-tetramethyl-4-bora-3a,4a-diaza-*s*-indacene)-3-bis(thiosemicarbazone), H$_2$L^1. *p*-NO$_2$-BODIPY (550 mg, 1.31 mmol) was dissolved in EtOH/CH$_2$Cl$_2$ (50:50, 50 mL) in the presence of 10% Pd/C (50 mg) and sparged with N$_{2(g)}$ and then H$_{2(g)}$. The reaction was stirred at room temperature under H$_{2(g)}$ (1 atm) for 16 h, after which reduction was complete (TLC: CH$_2$Cl$_2$). The Pd/C was removed via filtration through Celite into a RB flask, and the Celite was repeatedly washed with EtOH (3 × 5 mL). Atsmm$_2$ (340 mg, 1.31 mmol) was added to the filtrate, which was degassed and then refluxed for 16 h. On cooling to room temperature, an orange precipitate was collected, washed with ether, and air-dried (185 mg). The filtrate was concentrated by half and refluxed for a further 24 h, forming a second batch of orange precipitate, which was isolated in the same manner as the first (254 mg). The second batch was analytically identical to the first and combined to give a final yield of 60%. ^{1}H NMR (500 MHz; DMSO-d_6): δ/ppm 10.69 (s, 1H, N-N*H*-C═S), 10.31 (s, 1H, N-N*H*-C═S), 10.12 (s, 1H, Ar-N*H*-C═S), 8.44−8.41 (m, 1H, CH$_3$-N*H*-C═S), 7.85−7.84 (m, AA′BB′, 2H, ArH), 7.37−7.34 (m, AA′BB′, 2H, ArH), 6.19 (s, 2H, ArH), 3.04−3.03 (m, 3H, NH-C*H*$_3$), 2.45 (s, 6H, ArC*H*$_3$), 2.30 (s, 3H, N═C-C*H*$_3$), 2.28 (s, 3H, N═C-C*H*$_3$), 1.45 (s, 6H, ArC*H*$_3$). ^{13}C{^{1}H} NMR (125.7 MHz; DMSO-d_6): δ/ppm 178.5 (C═S), 176.7 (C═S), 154.8 (PyC), 149.6 (C═N-N), 147.7 (C═N-N), 142.8 (Ar-C-Py), 141.8 (PyC), 139.9 (ArC), 130.8 (PyC), 130.6 (ArC), 127.7 (ArCH), 125.5 (ArCH), 121.4 (PyCH), 31.2 (NH-*C*H$_3$), 14.3 (Py-*C*H$_3$), 14.2 (Py-*C*H$_3$), 12.2 (N═C-*C*H$_3$), 11.9 (N═C-*C*H$_3$). ^{19}F NMR (471 MHz; DMSO-d_6): δ/ppm −141.46 (dq, $^1J_{B,F}$ = 32 Hz, 2F, BF$_2$). MS(ES$^+$): *m*/*z* (calcd) 569.2247 (569.2174) {M + H$^+$}. HPLC: t_R 16.08 min. Crystals suitable for single-crystal X-ray diffraction were grown from dimethyl sulfoxide by slow vapor diffusion of atmospheric water at room temperature.

Diacetyl-4-methyl-4′-(8-(4-aminophenyl)-4,4-difluoro-1,3,5,7-tetramethyl-4-bora-3a,4a-diaza-*s*-indacene)-3-bis(thiosemicarbazonato)zinc(II), Zn^{II}L^1. H$_2$L^1 (80 mg, 0.14 mmol) was suspended in acetonitrile (20 mL) and heated to reflux. On addition of zinc(II) acetate (34 mg, 0.15 mmol), the suspension rapidly dissolved, and 15−20 min later, an orange precipitate began to appear. On stirring for a further 2 h the reaction was cooled to room temperature and the precipitate collected, washed repeatedly with diethyl ether, and dried *in vacuo* to give a bright red/orange solid (60 mg, 68%). ^{1}H NMR (500 MHz; DMSO-d_6): δ/ppm 9.60 (s, 1H, Ar-N*H*-C═S), 8.02−8.00 (m, AA′BB′, 2H, ArH), 7.40 (m, 1H, CH$_3$-N*H*-C═S), 7.21−7.19 (m, AA′BB′, 2H, ArH), 6.17 (s, 2H, ArH), 2.87 (m, 3H, NH-C*H*$_3$), 2.44 (s, 6H, ArC*H*$_3$), 2.32 (s, 3H, N═C−C*H*$_3$), 2.25 (s, 3H, N═C-C*H*$_3$), 1.44 (s, 6H, ArC*H*$_3$). ^{13}C{^{1}H} NMR (125.7 MHz; DMSO-d_6): δ/ppm 154.4 (Ar*C*), 149.8 (*C*═N−N), 144.6 (*C*═N-N), 142.7 (ArC), 142.5 (C), 142.0 (ArC), 131.1 (ArC), 127.9 (Ar*C*H), 126.3 (ArC), 121.2 (Ar*C*H), 119.9 (Ar*C*H), 14.9 (N═C-*C*H$_3$), 14.2 (Ar-*C*H$_3$), 14.2 (Ar-*C*H$_3$), 13.8 (N═C-*C*H$_3$). MS(ES$^+$): *m*/*z* (calcd) 631.1391 (631.1309) {M + H$^+$}. HPLC: t_R 16.08 min. Crystals suitable for single-crystal X-ray diffraction were grown from dimethyl sulfoxide by slow vapor diffusion of atmospheric water at room temperature.

Diacetyl-4-methyl-4′-(8-(4-aminophenyl)-4,4-difluoro-1,3,5,7-tetramethyl-4-bora-3a,4a-diaza-*s*-indacene)-3-bis(thiosemicarbazonato)copper(II), Cu^{II}L^1. H$_2$L^1 (80 mg, 0.14 mmol) was suspended in acetonitrile (20 mL) and heated to reflux. On addition of zinc(II) acetate (34 mg, 0.17 mmol), the suspension rapidly dissolved, and 10 min later, copper(II) acetate (37 mg, 0.17 mmol) was charged into the reaction vessel, resulting in rapid darkening of the solution. On stirring for a further 2 h the reaction was cooled to room temperature and the precipitate collected, washed repeatedly with diethyl ether, and dried *in vacuo* to give a dark red/brown solid (72 mg, 82%). MS(ES$^+$): *m*/*z* (calcd) 630.1399 (630.1314) {M + H$^+$}. HPLC: t_R 16.49 min. Crystals suitable for single-crystal X-ray diffraction were grown from dimethylformamide by slow vapor diffusion of atmospheric water at room temperature.

Fluorescence Decay Characterization Studies. The excitation beam (490 nm) was selected, using a prism/slit arrangement from a Fianium SC450-PP-HE Supercontinuum laser source producing pulses of ∼100 ps duration and at 2 MHz repetition rate.[69] The polarization of this excitation beam (output power ∼0.5 mW) was tidied up by passing it through a calcite rhomb polarizer to excite the sample with vertically polarized light. A monochromator (Jobin Yvon H-10) was used to isolate the emission, which was detected using a microchannel plate photomultiplier tube (Eldy model EM1-132-1) coupled to a PC card-based TCSPC electronics system (Edinburgh Instruments TCC900).

FLIM. Using the same laser source as the bulk solution measurements, the beam was delivered via a single-mode optical fiber to a modified Olympus confocal scanning microscope (FV300/IX71) coupled with a Becker & Hickl SPC-830 FLIM module. Confocally isolated emission was passed through a broad bandpass filter to block scattered excitation light and detected using a PMC-100 single photon counting photomultiplier, and data were acquired by an SPC-830 TCSPC card controlled using the SPCM operating software. The fluorescence decay data were analyzed using "SPCImage" FLIM data analysis software. Other details are as reported.[70]

DOI: 10.1021/acs.inorgchem.5b01599
Inorg. Chem. 2015, 54, 9556−9567

Cell Culture. All reagents were obtained from Life Technologies and used as received unless otherwise stated. M17 neuroblastoma cells were grown in culture, in Opti Mem medium supplemented with fetal bovine serum (10%), Gibco MEM nonessential amino acids (1%), and sodium pyruvate (100 μM). Cells were grown in a 37 °C, 5% CO_2 incubator to confluency prior to passaging. Cells were detached using trypsin/EDTA. Cells were seeded at 5×10^4 cells/cm^2 into a 35 mm Ibidi live cell imaging microdish and grown in culture for 24 h prior to treatment. Primary cortical neurons were harvested from C57 Black 6 mice. Prior to the use of primary murine cell cultures, ethics approval was obtained from the Biomedical Sciences Animal Ethics Committee, Ethics ID: 1011753, The University of Melbourne. Cortices were isolated from mouse fetuses at embryonic day 14 in Krebs solution, with added glucose (14 mM).

Cortices were subsequently incubated for 20 min at 37 °C in Krebs solution containing added trypsin (110 μM, Sigma). The solution was then centrifuged for 3 min at 259 RCF. After supernatant was removed, Krebs solution (10 mL) with DNase (25.8 nM) and STBI (129.38 nM Sigma) was added to the pellet and incubated for 2 min. Cells were then resuspended. The suspension was further centrifuged at 259 RCF for 3 min, supernatant was removed, and cells were resuspended in cortical plating medium comprising 10% 10× MEM, L-glutamine (1 μM), $NaHCO_3$ (50 mM), fetal bovine serum (10%), and horse serum (5%). Cells were plated at a density of 6×10^4 cells/cm^2 in an Ibidi 35 mm live cell imaging dish coated with 20 μg/mL poly-D-lysine. Cells were incubated at 37 °C for 24 h; then plating medium was replaced with Neurobasal medium supplemented with 2% B-27 supplement and L-glutamine (500 μM). After 5 days in culture at 37 °C, 5% CO_2, half of the medium was replaced. Cells were used for experiments after 8 days in culture.

Cell Treatments. Cells were treated with compounds (25 μM) and cotreated with combinations of molecular probes (Life Technologies). Concentrations of the molecular probes were as follows: LysoTracker red (1 μM), MitoTracker far red (2 μM), and HCS LipidTOX deep red neutral lipid stain (2 μM). After incubation for 1 h, the medium was removed and replaced with HEPES live cell imaging buffer. Confocal images were attained using a Leica SP5 confocal microscope, with LAS AF (Leica) software.

■ ASSOCIATED CONTENT

Ⓢ Supporting Information

The Supporting Information is available free of charge on the ACS Publications website at DOI: 10.1021/acs.inorgchem.5b01599.

Crystallographic data for $H_2\mathbf{L}^1$ (CIF)
Crystallographic data for $Zn^{II}\mathbf{L}^1$ (CIF)
Crystallographic data for $Cu^{II}\mathbf{L}^1$ (CIF)
Fluorescence decay data and curve fits for **L**, $Cu^{II}\mathbf{L}^1$, and $Zn^{II}\mathbf{L}^1$ (PDF)

■ AUTHOR INFORMATION

Corresponding Authors

*E-mail (A. R. White): arwhite@unimelb.edu.au. Fax: +61 3 8344 4004. Tel: +61 3 8344 1805.
*E-mail (T. A. Smith): trevoras@unimmelb.edu.au. Tel: +61 3 8344 6272.
*E-mail (P. S. Donnelly): pauld@unimelb.edu.au. Tel: +61 3 8344 2399.

Author Contributions

⊥J. L. Hickey and J. L. James contributed equally.

Funding

Australian Research Council, National and Health and Medical Research Council (Australia). P.S.D. is an ARC Future Fellow.

Notes

The authors declare no competing financial interest.

■ ACKNOWLEDGMENTS

Prof. Kevin Barnham (University of Melbourne) is acknowledged for his pivotal role in initiating our research in this area and the insight he continues to provide. We acknowledge Prof. Xiaotao Hao and Dr. Lachlan McKimmie for assistance with some of the FLIM measurements, and Prof. Andrew F. Hill (La Trobe University, Australia) for guidance on live-cell imaging studies. We acknowledge the Biological Optical Microscopy Platform (BOMP), University of Melbourne, for use of the confocal live cell microscopes.

■ REFERENCES

(1) French, F. A.; Freelander, B. L. *Cancer Res.* **1958**, *18*, 1290.
(2) Paterson, B. M.; Donnelly, P. S. *Chem. Soc. Rev.* **2011**, *40*, 3005.
(3) Green, M. A.; Klippenstein, D. L.; Tennison, J. R. *J. Nucl. Med.* **1988**, *29*, 1549.
(4) Green, M. A.; Mathias, C. J.; Welch, M. J.; McGuire, A. H.; Perry, D.; Fernandez-Rubio, F.; Perlmutter, J. S.; Raichle, M. E.; Bergmann, S. R. *J. Nucl. Med.* **1990**, *31*, 1989.
(5) Donnelly, P. S. *Dalton Trans.* **2011**, *40*, 999.
(6) Fujibayashi, Y.; Taniuchi, H.; Yonekura, Y.; Ohtani, H.; Konishi, J.; Yokoyama, A. *J. Nucl. Med.* **1997**, *38*, 1155.
(7) Tanaka, T.; Furukawa, T.; Fujieda, S.; Kasamatsu, S.; Yonekura, Y.; Fujibayashi, Y. *Nucl. Med. Biol.* **2006**, *33*, 743.
(8) Lewis, J. S.; Laforest, R.; Dehdashti, F.; Grigsby, P. W.; Welch, M. J.; Siegel, B. A. *J. Nucl. Med.* **2008**, *49*, 1177.
(9) Vavere, A. L.; Lewis, J. S. *Dalton Trans.* **2007**, 4893.
(10) Fujibayashi, Y.; Cutler, C. S.; Anderson, C. J.; McCarthy, D. W.; Jones, L. A.; Sharp, T.; Yonekura, Y.; Welch, M. J. *Nucl. Med. Biol.* **1999**, *26*, 117.
(11) Basken, N. E.; Green, M. A. *Nucl. Med. Biol.* **2009**, *36*, 495.
(12) Haynes, N. G.; Lacy, J. L.; Nayak, N.; Martin, C. S.; Dai, D.; Mathias, C. J.; Green, M. A. *J. Nucl. Med.* **2000**, *41*, 309.
(13) Dearling, J. L. J.; Lewis, J. S.; McCarthy, D. W.; Welch, M. J.; Blower, P. J. *Chem. Commun.* **1998**, 2531.
(14) Dearling, J. L. J.; Lewis, J. S.; Mullen, G. D.; Welch, M. J.; Blower, P. J. *JBIC, J. Biol. Inorg. Chem.* **2002**, *7*, 249.
(15) Xiao, Z.; Donnelly, P. S.; Zimmermann, M.; Wedd, A. G. *Inorg. Chem.* **2008**, *47*, 4338.
(16) Donnelly, P. S.; Caragounis, A.; Du, T.; Laughton, K. M.; Volitakis, I.; Cherny, R. A.; Sharples, R. A.; Hill, A. F.; Li, Q.-X.; Masters, C. L.; Barnham, K. J.; White, A. R. *J. Biol. Chem.* **2008**, *283*, 4568.
(17) Crouch, P. J.; Hung, L. W.; Adlard, P. A.; Cortes, M.; Lal, V.; Filiz, G.; Perez, K. A.; Nurjono, M.; Caragounis, A.; Du, T.; Laughton, K.; Volitakis, I.; Bush, A. I.; Li, Q.-X.; Masters, C. L.; Cappai, R.; Cherny, R. A.; Donnelly, P. S.; White, A. R.; Barnham, K. J. *Proc. Natl. Acad. Sci. U. S. A.* **2009**, *106*, 381.
(18) Fodero-Tavoletti, M. T.; Villemagne, V. L.; Paterson, B. M.; White, A. R.; Li, Q.-X.; Camakaris, J.; O'Keefe, G.; Cappai, R.; Barnham, K. J.; Donnelly, P. S. *J. Alzheimer's Dis.* **2010**, *20*, 49.
(19) Hung, L. W.; Villemagne, V. L.; Cheng, L.; Sherratt, N. A.; Ayton, S.; White, A. R.; Crouch, P. J.; Lim, S.; Leong, S. L.; Wilkins, S.; George, J.; Roberts, B. R.; Pham, C. L. L.; Liu, X.; Chiu, F. C. K.; Shackleford, D. M.; Powell, A. K.; Masters, C. L.; Bush, A. I.; O'Keefe, G.; Culvenor, J. G.; Cappai, R.; Cherny, R. A.; Donnelly, P. S.; Hill, A. F.; Finkelstein, D. I.; Barnham, K. J. *J. Exp. Med.* **2012**, *209*, 837.
(20) Roberts, B. R.; Turner, B. J.; Bush, A. I.; Masters, C. L.; Li, Q.-X.; Lim, N. K. H.; McAllum, E. J.; Price, K. A.; Kanninen, K. M.; Liddell, J. R.; Grubman, A.; Donnelly, P. S.; Lim, S.; Paterson, B. M.; Hickey, J. L.; Hare, D. J.; Doble, P. A.; Rhoads, T. W.; Williams, J. R.; Hung Lin, W.; Monty, J.-F.; Llanos, R. M.; Mercer, J. F. B.; Kramer, D. R.; Duce, J. A.; Beckman, J. S.; Barnham, K. J.; White, A. R.; Crouch, P. J. *J. Neurosci.* **2014**, *34*, 8021.
(21) Soon, C. P. W.; Donnelly, P. S.; Turner, B. J.; Hung, L. W.; Crouch, P. J.; Sherratt, N. A.; Tan, J. L.; Lim, N. K. H.; Lam, L.; Bica, L.; Lim, S. C.; Hickey, J. L.; Morizzi, J.; Powell, A.; Finkelstein, D. I.;

DOI: 10.1021/acs.inorgchem.5b01599
Inorg. Chem. 2015, 54, 9556−9567

Culvenor, J. G.; Masters, C. L.; Duce, J.; White, A. R.; Barnham, K. J.; Li, Q. X. *J. Biol. Chem.* **2011**, *286*, 44035.
(22) McAllum, E. J.; Lim, N. K. H.; Hickey, J. L.; Paterson, B. M.; Donnelly, P. S.; Li, Q.-X.; Liddell, J. R.; Barnham, K. J.; White, A. R.; Crouch, P. J. *Amyotrophic Lateral Scler. Frontotemporal Degener.* **2013**, *14*, 586.
(23) Cowley, A. R.; Davis, J.; Dilworth, J. R.; Donnelly, P. S.; Dobson, R.; Nightingale, A.; Peach, J. M.; Shore, B.; Kerr, D.; Seymour, L. *Chem. Commun.* **2005**, 845.
(24) Dayal, D.; Palanimuthu, D.; Shinde, S. V.; Somasundaram, K.; Samuelson, A. G. *JBIC, J. Biol. Inorg. Chem.* **2011**, *16*, 621.
(25) Palanimuthu, D.; Shinde, S. V.; Dayal, D.; Somasundaram, K.; Samuelson, A. G. *Eur. J. Inorg. Chem.* **2013**, *2013*, 3542.
(26) Pascu, S. I.; Waghorn, P. A.; Conry, T. D.; Betts, H. M.; Dilworth, J. R.; Churchill, G. C.; Pokrovska, T.; Christlieb, M.; Aigbirhio, F. I.; Warren, J. E. *Dalton Trans.* **2007**, 4988.
(27) Pascu, S. I.; Waghorn, P. A.; Conry, T. D.; Lin, B.; Betts, H. M.; Dilworth, J. R.; Sim, R. B.; Churchill, G. C.; Aigbirhio, F. I.; Warren, J. E. *Dalton Trans.* **2008**, 2107.
(28) Pascu, S. I.; Waghorn, P. A.; Kennedy, B. W. C.; Arrowsmith, R. L.; Bayly, S. R.; Dilworth, J. R.; Christlieb, M.; Tyrrell, R. M.; Zhong, J.; Kowalczyk, R. M.; Collison, D.; Aley, P. K.; Churchill, G. C.; Aigbirhio, F. I. *Chem. - Asian J.* **2010**, *5*, 506.
(29) Lim, S.; Price, K. A.; Chong, S.-F.; Paterson, B. M.; Caragounis, A.; Barnham, K. J.; Crouch, P. J.; Peach, J. M.; Dilworth, J. R.; White, A. R.; Donnelly, P. S. *JBIC, J. Biol. Inorg. Chem.* **2010**, *15*, 225.
(30) Price, K. A.; Crouch, P. J.; Lim, S.; Paterson, B. M.; Liddell, J. R.; Donnelly, P. S.; White, A. R. *Metallomics* **2011**, *3*, 1280.
(31) Baggaley, E.; Botchway, S. W.; Haycock, J. W.; Morris, H.; Sazanovich, I. V.; Williams, J. A. G.; Weinstein, J. A. *Chem. Sci.* **2014**, *5*, 879.
(32) Baggaley, E.; Gill, M. R.; Green, N. H.; Turton, D.; Sazanovich, I. V.; Botchway, S. W.; Smythe, C.; Haycock, J. W.; Weinstein, J. A.; Thomas, J. A. *Angew. Chem., Int. Ed.* **2014**, *53*, 3367.
(33) Renfrew, A. K.; Bryce, N. S.; Hambley, T. W. *Chem. Sci.* **2013**, *4*, 3731.
(34) Arrowsmith, R. L.; Waghorn, P. A.; Jones, M. W.; Bauman, A.; Brayshaw, S. K.; Hu, Z.; Kociok-Koehn, G.; Mindt, T. L.; Tyrrell, R. M.; Botchway, S. W.; Dilworth, J. R.; Pascu, S. I. *Dalton Trans.* **2011**, *40*, 6238.
(35) Ulrich, G.; Ziessel, R.; Harriman, A. *Angew. Chem., Int. Ed.* **2008**, *47*, 1184.
(36) Ziessel, R.; Bonardi, L.; Ulrich, G. *Dalton Trans.* **2006**, 2913.
(37) Loudet, A.; Burgess, K. *Chem. Rev.* **2007**, *107*, 4891.
(38) Waghorn, P. A.; Jones, M. W.; Theobald, M. B. M.; Arrowsmith, R. L.; Pascu, S. I.; Botchway, S. W.; Faulkner, S.; Dilworth, J. R. *Chem. Sci.* **2013**, *4*, 1430.
(39) Biedler, J. L.; Roffler-Tarlov, S.; Schachner, M.; Freedman, L. S. *Cancer Res.* **1978**, *38*, 3751.
(40) Fischer, H. *Organic Syntheses*; Wiley: New York, 1935; Vol. *XV*, p 20
(41) Fischer, H. *Organic Syntheses*; Wiley: New York, 1935; Vol. *XV*, p 17
(42) Paterson, B. M.; Karas, J. A.; Scanlon, D. B.; White, J. M.; Donnelly, P. S. *Inorg. Chem.* **2010**, *49*, 1884.
(43) Buncic, G.; Donnelly, P. S.; Paterson, B. M.; White, J. M.; Zimmermann, M.; Xiao, Z.; Wedd, A. G. *Inorg. Chem.* **2010**, *49*, 3071.
(44) Azov, V. A.; Diederich, F.; Lill, Y.; Hecht, B. *Helv. Chim. Acta* **2003**, *86*, 2149.
(45) Azov, V. A.; Skinner, P. J.; Yamakoshi, Y.; Seiler, P.; Gramlich, V.; Diederich, F. *Helv. Chim. Acta* **2003**, *86*, 3648.
(46) Cowley, A. R.; Dilworth, J. R.; Donnelly, P. S.; Labisbal, E.; Sousa, A. *J. Am. Chem. Soc.* **2002**, *124*, 5270.
(47) Blower, P. J.; Castle, T. C.; Cowley, A. R.; Dilworth, J. R.; Donnelly, P. S.; Labisbal, E.; Sowrey, F. E.; Teat, S. J.; Went, M. J. *Dalton Trans.* **2003**, 4416.
(48) Holland, J. P.; Aigbirhio, F. I.; Betts, H. M.; Bonnitcha, P. D.; Burke, P.; Christlieb, M.; Churchill, G. C.; Cowley, A. R.; Dilworth, J. R.; Donnelly, P. S.; Green, J. C.; Peach, J. M.; Vasudevan, S. R.; Warren, J. E. *Inorg. Chem.* **2007**, *46*, 465.
(49) Holland, J. P.; Green, J. C.; Dilworth, J. R. *Dalton Trans.* **2006**, 783.
(50) Martin, S.; Parton, R. G. *Nat. Rev. Mol. Cell Biol.* **2006**, *7*, 373.
(51) Farese, R. V., Jr.; Walther, T. C. *Cell* **2009**, *139*, 855.
(52) Guo, Y.; Cordes, K. R.; Farese, R. V., Jr.; Walther, T. C. *J. Cell Sci.* **2009**, *122*, 749.
(53) Granneman, J. G.; Moore, H.-P. H.; Mottillo, E. P.; Zhu, Z. *J. Biol. Chem.* **2009**, *284*, 3049.
(54) Singh, R.; Kaushik, S.; Wang, Y.; Xiang, Y.; Novak, I.; Komatsu, M.; Tanaka, K.; Cuervo, A. M.; Czaja, M. J. *Nature* **2009**, *458*, 1131.
(55) Brotherus, J.; Renkonen, O. *J. Lipid Res.* **1977**, *18*, 191.
(56) Matsumoto, K.; Fujibayashi, Y.; Arano, Y.; Wada, K.; Yokoyama, A. *Nucl. Med. Biol.* **1992**, *19*, 33.
(57) Petering, D. H. *Biochem. Pharmacol.* **1974**, *23*, 567.
(58) Donnelly, P. S.; Liddell, J. R.; Lim, S.; Paterson, B. M.; Cater, M. A.; Savva, M. S.; Mot, A. I.; James, J. L.; Trounce, I. A.; White, A. R.; Crouch, P. J. *Proc. Natl. Acad. Sci. U. S. A.* **2012**, *109*, 47.
(59) Yoshii, Y.; Yoneda, M.; Ikawa, M.; Furukawa, T.; Kiyono, Y.; Mori, T.; Yoshii, H.; Oyama, N.; Okazawa, H.; Saga, T.; Fujibayashi, Y. *Nucl. Med. Biol.* **2012**, *39*, 177.
(60) Liu, L.; Zhang, K.; Sandoval, H.; Yamamoto, S.; Jaiswal, M.; Sanz, E.; Li, Z.; Hui, J.; Graham, B. H.; Quintana, A.; Bellen, H. J. *Cell* **2015**, *160*, 177.
(61) Sanhueza, M.; Chai, A.; Smith, C.; McCray, B. A.; Simpson, T. I.; Taylor, J. P.; Pennetta, G. *PLoS Genet.* **2015**, *11*, e1005107.
(62) Wada, K.; Yasuhisa; Tajima, N.; Naoyuki; Yokoyama, A.; Akira; Fujibayashi, Y. *Biol. Pharm. Bull.* **1994**, *17*, 701.
(63) Fahrni, C. J. *Curr. Opin. Chem. Biol.* **2013**, *17*, 656.
(64) Cotruvo, J. A., Jr.; Aron, A. T.; Ramos-Torres, K. M.; Chang, C. J. *Chem. Soc. Rev.* **2015**, *44*, 4400.
(65) Shen, C.; New, E. J. *Metallomics* **2015**, *7*, 56.
(66) Price, K. A.; Hickey, J. L.; Xiao, Z.; Wedd, A. G.; James, S. A.; Liddell, J. R.; Crouch, P. J.; White, A. R.; Donnelly, P. S. *Chem. Sci.* **2012**, *3*, 2748.
(67) Sheldrick, G. M. *Acta Crystallogr., Sect. A: Found. Crystallogr.* **2008**, *64*, 112.
(68) Farrugia, L. J. *J. Appl. Crystallogr.* **2012**, *45*, 849.
(69) Wildanger, D.; Rittweger, E.; Kastrup, L.; Hell, S. W. *Opt. Express* **2008**, *16*, 9614.
(70) Hao, X.-T.; McKimmie, L. J.; Smith, T. A. *J. Phys. Chem. Lett.* **2011**, *2*, 1520.

DOI: 10.1021/acs.inorgchem.5b01599
Inorg. Chem. 2015, 54, 9556−9567